Biomass Conversion and Biorefinery
https://doi.org/10.1007/s13399-024-05840-7

ORIGINAL ARTICLE

Adsorptive removal of hazardous rhodamine B dye from aqueous solutions by St. John's wort (*Hypericum perforatum*)

Birol Isik[1]

Received: 1 March 2024 / Revised: 26 May 2024 / Accepted: 4 June 2024

Abstract

In this work, it was aimed to remove the highly toxic rhodamine B (RhB) dye from wastewater by using a low-cost, renewable, sustainable, and completely natural adsorbent obtained from St. John's wort (*Hypericum perforatum*) (HP), which is considered an agro-waste. HP was characterized by FTIR-ATR, XRD, FESEM, and pH_{pzc}. Adsorption experiments were conducted by optimizing pH (2–12), dose (0.01–0.30 g), time (0–120 min), and concentration (10–50 mg/L). Equilibrium data were applied to linear isotherms. The results stated that the removal process occurred in a monolayer on the homogeneous surface of HP and the q_m value was determined as 196.08 mg/g at 298 K. Kinetic results showed that RhB adsorption on HP followed a quasi-second-order. The effect of salt concentration onto RhB adsorption on HP adsorbent and reusability studies were conducted. Thermodynamic tests showed that the process was exothermic ($\Delta H_A^o = -13.58 kJ/mol$) and spontaneous ($\Delta G_A^o = -26.61 kJ/mol$). The results of the study indicated that HP may be a favorable adsorbent for basic dyes in wastewater.

Keywords Adsorption · Agro-waste · St. John's wort · Rhodamine B

1 Introduction

The rapid expansion and growth of industrial, technological, and scientific activity increase human population and globalization, which, while providing many benefits, can also bring many difficulties for the overall ecosystem [1, 2]. The wastes produced by this process constitute a significant hazard to the atmosphere and terrestrial and aquatic habitats. In recent years, contaminants created during the manufacturing process in numerous industries such as textile, food, cosmetics, automobile, paper, and others have been mixed into groundwater, reducing water quality and causing significant harm to the living population. These wastes dumped into groundwater comprise a variety of hazardous, poisonous, and non-biodegradable components that pollute the ecosystem [3, 4].

The textile sector consumes a large quantity of water during production and discharges wastewater from textile dyes, which are among the biggest pollutants, into groundwater. Textile dyes are well-known to be exceedingly hazardous to human health and the aquatic habitat [5]. Additionally, dyes interfere with photosynthetic activities by blocking sunlight from reaching aquatic environments, which has a negative influence on aquatic ecology [6]. Among textile dyes, azo dyes are numerous and account for 50% of annual output. Rhodamine B (RhB) dye, one of the most poisonous dyes found in textile wastewater, is commonly employed as a colorant in the textile sector because of its great stability and biodegradability. RhB dye is often used in ballpoint pens, paints, leather, paint lasers, carbon plates, stamp pad inks, crackers, and explosives [7–9]. Since RhB dye is a water-soluble dye, it can have negative impacts on the aquatic ecosystem. Furthermore, when RhB dye is released into the watery environment, it reduces light penetration, making photosynthesis more difficult and, as a result, lowering oxygen levels in the water, resulting in the decline or extinction of aquatic life. As a result, before being discharged into the aquatic environment, such dyes should be disposed of [10–12].

In recent years, various physicochemical techniques such as reverse osmosis, adsorption, ion exchange, solvent extraction, chemical oxidation, electrocoagulation, and coagulation-flocculation have been used for the treatment of wastewater containing dyes [13]. Among these techniques, adsorption is preferred more than other techniques due to its advantages such as simplicity, naturalness, low cost, and high efficiency. The capacity of adsorbents used in

---

✉ Birol Isik
19birol91@gmail.com

[1] Department of Chemistry, Faculty of Arts & Sciences, Yildiz Technical University, Esenler, Istanbul 34220, Turkey

the adsorption technique to remove various pollutants determines the efficiency of the adsorption process [14–16]. Various adsorbents such as polymers [17], composites [18], clays [19], activated carbon [20], nanomaterials [21], and natural plants [22] are used in the adsorption process.

Agro-waste biomaterials are environmentally beneficial, affordable, low-density, and have equivalent mechanical qualities [23]. Among these biomaterials, the St. John's wort plant, whose Latin name is *Hypericum perforatum* L. (HP), is a plant belonging to the Hypericaceae family. Traditionally, it is widely used as herbal tea or food supplement. It contains many chemical compounds that may show pharmacological and biochemical activity. In addition, it can also show antidepressant properties due to chemicals such as naphthodianthrones, hypericin, and pseudo-hypericin [24–26].

HP is a cheap and abundant natural plant that can be used in various fields, making it a suitable option for adsorption, which has not yet been reported in the literature. The present study aimed to achieve effective and rapid removal of RhB dye from wastewater using an adsorbent derived from this plant. The influence of various parameters on the removal process was studied, and equilibrium, kinetic, and thermodynamic tests were conducted.

2 Materials and methods

Table 1 contains information about the study's resources. Without additional purification, all compounds were utilized. The chemical structure of RhB dye is presented in Fig. S1.

HP plants from herbalists in Istanbul, Turkey, were used as adsorbents in the context of agro-waste. The plants were properly cleaned with distilled water and allowed to air dry. Using a ball mill to grind the dried HP plants into < 100 mesh particles, they were then dried at 105 °C for 2 days. For use in removal experiments, they were thereafter kept in a desiccator.

A Nicolet IS10 Thermo FTIR-ATR spectrophotometer, Malvern PANalytical X'Pert PRO XRD, Thermo Scientific Apreo 2 S LoVac FESEM, and Ohaus Starter 3100 pH-meter were used to perform FTIR-ATR (Fourier transform-attenuated total reflectance), FESEM (field emission scanning electron microscope), XRD (X-ray diffractometer), and pH_{pzc} analyses. FTIR-ATR analyses were used to detect functional groups on the surface of HP and their changes pre- and post-removal. XRD analysis was used to determine the crystalline structure of HP. FESEM analyses were used to examine the morphology of HP and its changes pre- and post-adsorption. The point of zero charge (pH_{pzc}) tests were conducted from the solid addition technique [27, 28].

An individual batch system was used to study the removal process of RhB dye using HP. The experiments were conducted at constant stirring speed (120 rpm) and repeated three times to minimize error. The solution pH was adjusted with 0.1 M NaOH and 0.1 HCl solutions obtained from Sigma-Aldrich, and pH tests were conducted between 2 and 12. The concentration range in the experiments was chosen as 10–50 mg/L. At the end of the experiments, the samples were analyzed at 554 nm using a UV-vis spectrophotometer. The removal percentage of RhB dye and its capacity were determined according to Eqs. (S1) and (S2). Different isotherm and kinetic models were used for kinetic and equilibrium experiments, and the linear equations of these models were presented in Table 2. Furthermore, the accuracy and applicability of the kinetic and isotherm experiments were evaluated using five different error functions (SSE, ARE, RMSE, χ^2, and EABS). The equations of the error functions were also presented in the supporting information. Additionally, RhB removal tests at three different temperatures were carried out to look into the thermodynamics of the removal process [29–31].

3 Results and discussion

3.1 Characterization of HP

FTIR-ATR spectra of HP before and after the adsorption process are illustrated in Fig. 1. From the spectra, similar peaks were depicted. From the spectrum before adsorption, the peaks obtained at 3285, 2917, 2849, 1604, 1440, and 1023 cm^{-1} were assigned to -OH stretchings, C-H stretchings, C = O stretchings, C-H bendings, and C-O stretchings, respectively [26]. For the sample after adsorption, a similar spectrum was obtained that of before adsorption. Additionally, some of the peaks were observed to shift. These shifts were assigned to the electrostatic interactions between dye molecules and adsorbent surfaces.

Table 1 Chemicals used in this study

Chemicals	Formula	Source	Molecular weight	Assay	CAS No.
Rhodamine B	$C_{28}H_{31}ClN_2O_3$	Sigma-Aldrich	479.01	≥90.0%	81-88-9
Hydrochloric acid	HCl	Sigma-Aldrich	36.46	37.0%	7647-01-0
Sodium hydroxide	NaOH	Sigma-Aldrich	40.00	≥97.0%	1310-73-2
Calcium chloride	$CaCl_2$	Sigma-Aldrich	110.98	≥97.0%	10043-52-4
Sodium chloride	NaCl	Sigma-Aldrich	58.44	≥99.0%	7647-14-5
Sodium nitrate	$NaNO_3$	Sigma-Aldrich	84.99	≥99.0%	7631-99-4

Table 2 The equations and parameters of isotherm, kinetic, and thermodynamic used in this work

Description Isotherms	Equations	No.	Parameters
Freundlich	$lnq_e = lnK_F + \frac{1}{n} \times lnC_e$	(1)	K_F: Isotherm constant (L/mg) n: Freundlich constant indicating the adsorption intensity
Langmuir	$\frac{1}{q_e} = \frac{1}{q_m} + \frac{1}{K_L * q_m} \times \frac{1}{C_e}$	(2)	K_L: Isotherm constant (L/mg) q_m: Maximum adsorption capacity (mg/g)
D-R	$\ln(q_e) = \ln(q_{DR}) - \beta \times \epsilon^2$ $\epsilon = R \times T \times ln\left(1 + \frac{1}{C_e}\right)$ $E_{D-R} = (2 \times \beta)^{-0.5}$	(3) (4) (5)	q_{DR}: Theoretical sorption capacity (mg/g) E_{D-R}: Sorption energy (kJ/mol) ϵ: Polanyi potential β: Constant of sorption energy (mol^2/J^2) R: Ideal gas constant (J/molK) T: Ambient temperature (K)
Temkin	$q_e = \beta_T \ln K_T + \beta_T \ln C_e$ $\beta_T = RT/b_T$	(6) (7)	β_T: The Temkin constant linked with the heat of adsorption K_T: The equilibrium binding constant (L/g) corresponding to the maximum binding energy b_T: The Temkin constant (J/mol)
Kinetics			
Quasi-first-order	$\ln(q_e - q_t) = \ln q_e - k_1 t$	(8)	k_1: *Quasi-first-order* rate constant (min^{-1})
Quasi-second-order	$\frac{t}{q_t} = \frac{1}{k_2 q_e^2} + \frac{1}{q_e} \times t$	(9)	k_2: *Quasi-second-order* rate constant (g/mg.min)
Thermodynamics			
$\Delta G^o = -R \times T \times \ln K_e^o$		(10)	ΔG^o: Gibbs free energy, ΔH^o: Enthalpy, ΔS^o: Entropy
$\ln K_e^o = -\frac{\Delta G^o}{R \times T} = \frac{\Delta S^o}{R} - \frac{\Delta H^o}{R} \times \frac{1}{T}$		(11)	K_e^o: Thermodynamic equilibrium constant
$\ln K_e^o = \frac{1000 \times K_L \times M_{\mathrm{RhB}} \times [\mathrm{Adsorbate}]^o}{\gamma}$		(12)	M_{RhB}: Molecular weight of RhB dye, $[Adsorbate]^o$: Standard concentration of adsorptive molecules (1 mol/L), γ: Activity coefficient (dimensionless)
$\Delta G^o = \Delta H^o - T \times \Delta S^o$		(13)	T: Ambient temperature (K)

The XRD pattern of HP is shown in Fig. 2. HP's pattern consists of up of wide and sharp peaks localized between 2q = 10–30°, indicating its semicrystalline structure [32]. The peak at about 2q = 22° is assigned to the crystalline form of cellulose I. The range between 2q = 15° and 2q = 25° corresponds to the amorphous phases of lignin, hemicellulose, and cellulose [33].

The FESEM images of HP are presented in Fig. 3. Before dye removal, HP was found to have a cleft, rough, irregular, and complex surface suitable for RhB dye retention. After the removal of RhB dye from water, it was found that the

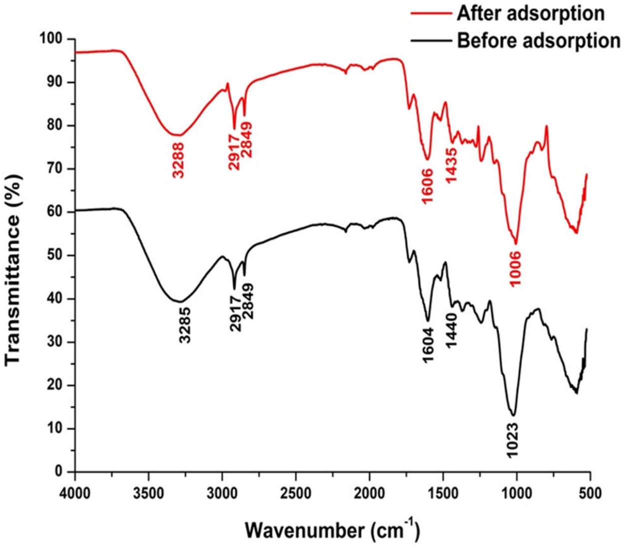

Fig. 1 The FTIR-ATR spectra of HP before and after RhB adsorption (wavenumber range: 500–4000 cm^{-1})

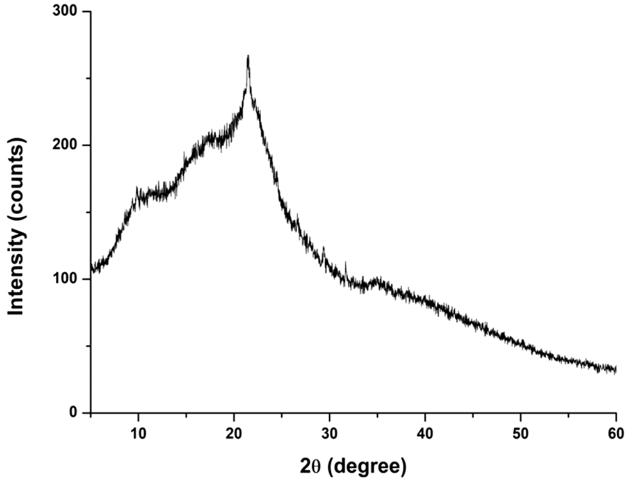

Fig. 2 The XRD pattern of HP (2q = 0–60 °C, 40 mA, 45 kV)

surface of HP became almost smooth and more consistent, and the dye covered the irregularities on the surface.

3.2 Influence of optimum conditions

Figure 4a depicts the relationship between the pH of the RhB solution and the removal percentage. From the results, it was observed that the percentage removal of RhB using HP increased from 33.96 to 73.83% as the solution pH increased from 2 to 7. After this value, it decreased slightly and increased to 80.03% at pH = 12. This is thought to be because of the electrostatic attraction between RhB and HP surface. In addition, the surface charge of HP was determined by pH_{pzc} analysis, and the results are illustrated in Fig. 5. The pH_{pzc} value of HP was calculated as 5.83. When the solution pH is above the pH_{pzc} value, the acidic oxygen groups on the surface of HP undergo deprotonation and the negative charge density on the surface enhances, which leads to an increase in the removal percentage of the cationic RhB dye. On the flip side of the coin, RhB dye exists in aqueous solutions in cationic and zwitterionic states. When the solution pH is above $pK_a = 3.7$, similarly, the carboxyl group of RhB dye undergoes deprotonation, which leads to the conversion of the cationic to the zwitterionic form. This leads to the emergence of electrostatic repulsion between RhB and negatively charged HP surface functional groups. If the solution pH is less than pH_{pzc}, the HP surface is protonated, increasing the positive charge density on the surface and causing an electrostatic repulsion force with the cationic RhB dye and diminishing the removal percentage [20, 34, 35].

It is of great importance to determine the optimum dose of HP for the effective removal of RhB dye from water. For this purpose, the HP dose was varied between 0.01 and 0.30 g, keeping other parameters constant. The results were presented in Fig. 4b. As a result, the optimal HP dose for maximum removal of RhB was 0.1 g, after which there was no significant increase in the removal percentage. The rapid reaching of reaction equilibrium is because of the high amount of accessible active parts on the surface at low HP doses. Similar results are also found in the literature [36, 37]. After 0.1 g HP dose, there was no significant increase as the surface-active sites were saturated with RhB molecules. At a dose of 0.1 g HP, the removal percentage reached approximately 86%. This result indicated that HP could be a potential adsorbent for wastewater treatment.

The influence of initial concentration on removal percentage and capacity was evaluated in the range of 10 to 50 mg/L, and the results are presented in Fig. 4c. The results showed that the adsorption capacity of RhB by HP was a function of initial RhB concentration and the removal percentage diminished with enhancing concentration. At low RhB concentrations, the ratio of the number of active sites of the HP to the available reactive sites of the RhB dye decreases and the possibility of interaction between them increases, thereby increasing the adsorption capacity [38].

The change in the removal percentage depending on the contact time between HP and RhB solution was analyzed in the range of 0–120 min, and the results are given in Fig. 4d. It was discovered that as the RhB solution and HP's contact duration lengthened, the elimination percentage rose. At the contact time of 45 min, the removal percentage of RhB on HP reached a maximum of 70.78%, 74.98%, and 77.68% for 298 K, 308 K, and 318 K, respectively. After 45 min, there was no significant change as the active parts reached saturation. These findings led to the calculation of a 45-min contact period for studies on equilibrium.

3.3 Adsorption isotherms

To comprehensively study the interactions between HP and RhB and the functioning of the process, isotherm models

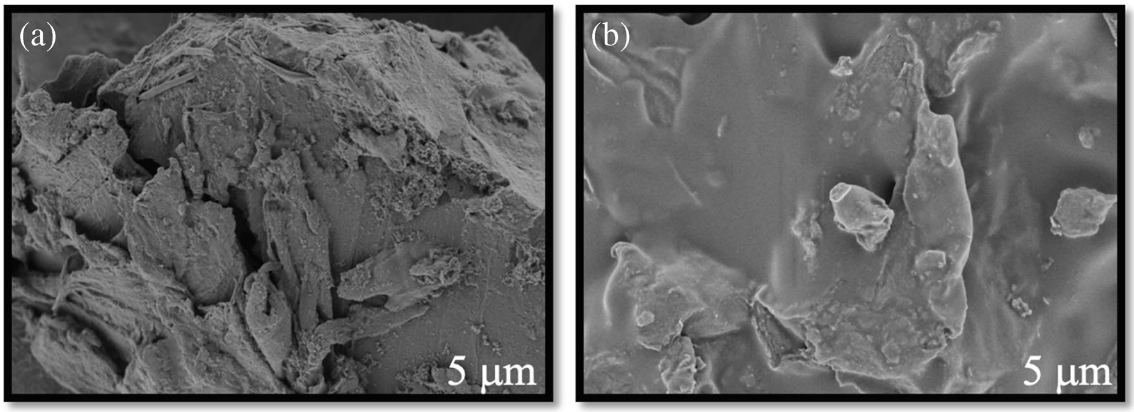

Fig. 3 The FESEM image of HP pre- (**a**) and post- (**b**) removal of RhB dye (particle size: 5 µm, magnification: 25.00 KX, electron high tension: 10.00 kV, and working distance: 2.82 mm)

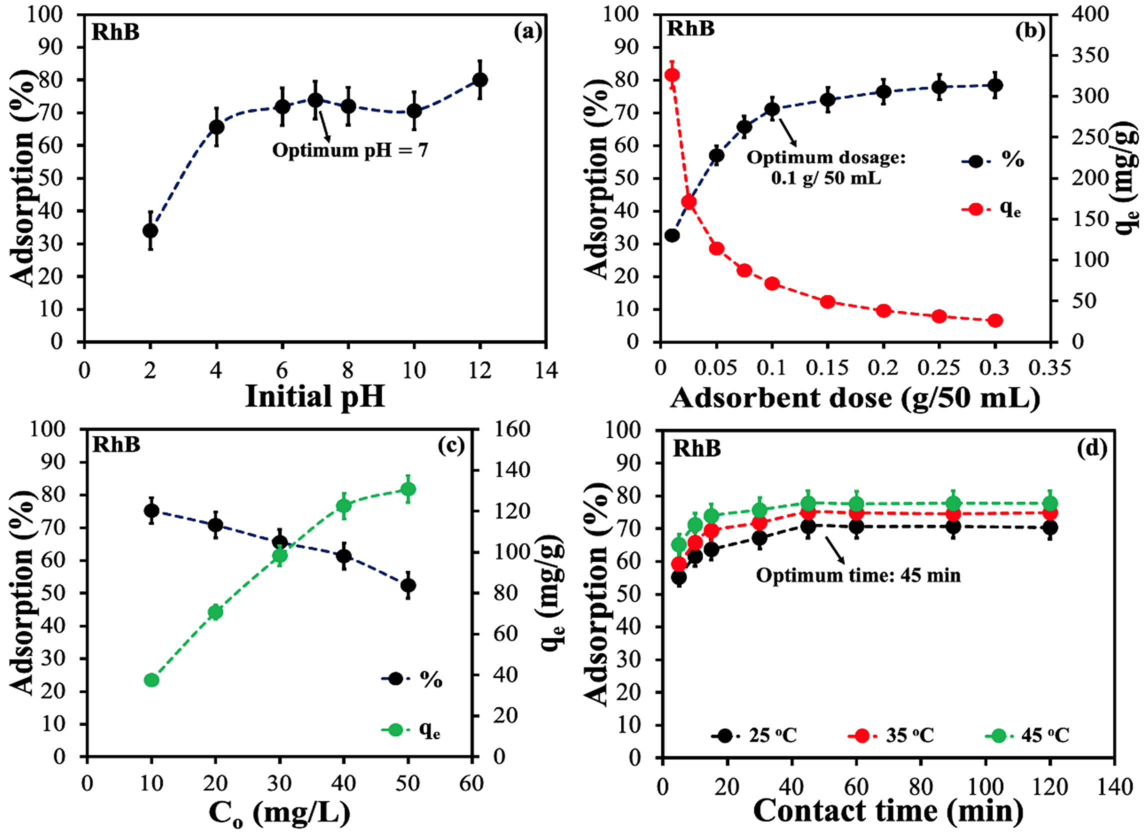

Fig. 4 The influence of optimum conditions: **a** initial pH (constant dosage: 0.1 g, volume: 50 mL, speed: 120 rpm, contact time: 45 min, concentration: 20 mg/L, temperature: 25 °C), **b** HP dose (contact time: 45 min, volume: 50 mL, speed: 120 rpm, pH ≅ 7, concentration: 20 mg/L, temperature: 25 °C), **c** RhB concentration (constant dosage: 0.1 g, volume: 50 mL, speed: 120 rpm, pH ≅ 7, contact time: 45 min, temperature: 25 °C), and **d**) ontact time (constant dosage: 0.1 g, volume: 50 mL, speed: 120 rpm, pH ≅ 7, concentration: 20 mg/L, temperature: 25 °C)

were applied to the adsorption process. The amount of RhB adsorbed on HP increases rapidly at low concentrations and gradually reaches a plateau at high concentrations (Fig. 6a) [39–41]. The raw data were applied to four different isotherms. The linear equations of the isotherm models are given in Table 2.

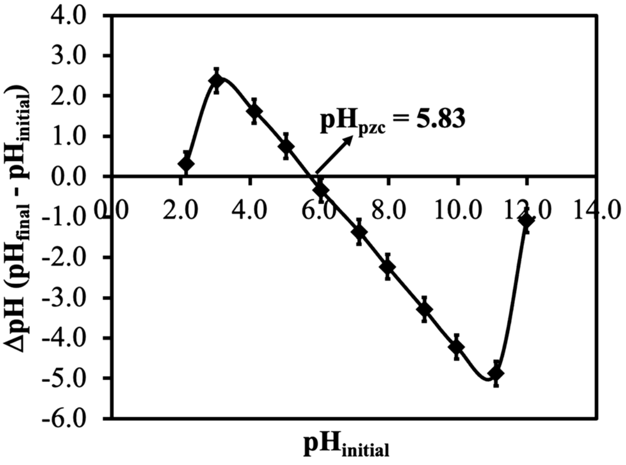

Fig. 5 The pH_{pzc} of HP (agitation speed: 120 rpm, contact time: 48 h, pH range: 2–12, volume: 50 mL, adsorbent dosage: 0.2 g)

The isotherm parameters and results obtained from the linear plots in Fig. 6 are presented in Table 3. In a comparison of the r^2 values of the Langmuir and Freundlich, it was found that the Langmuir isotherm had a greater correlation, indicating that this model matches the experimental data better. Furthermore, as seen from Table 3, the q_m value from Langmuir isotherm was determined as 196.08 mg/g at 298 K. The Langmuir hypothesis states that all active parts on the monolayer surface of HP have the same energy and that RhB molecules are anchored to homogenous areas of that surface [19, 42]. Table 4 shows the comparison of the removal capacity of HP for RhB with existing adsorbents in the literature. The D-R model was used to apply the experimental results to examine the nature of the interaction between the RhB molecule and the HP surface. According to this model, the process is physical if the E_{D-R} value is lower than 8 kJ/mol and chemical if the E_{D-R} value is greater than 8 kJ/mol [43–45]. As shown in Table 3, the E_{D-R} value was

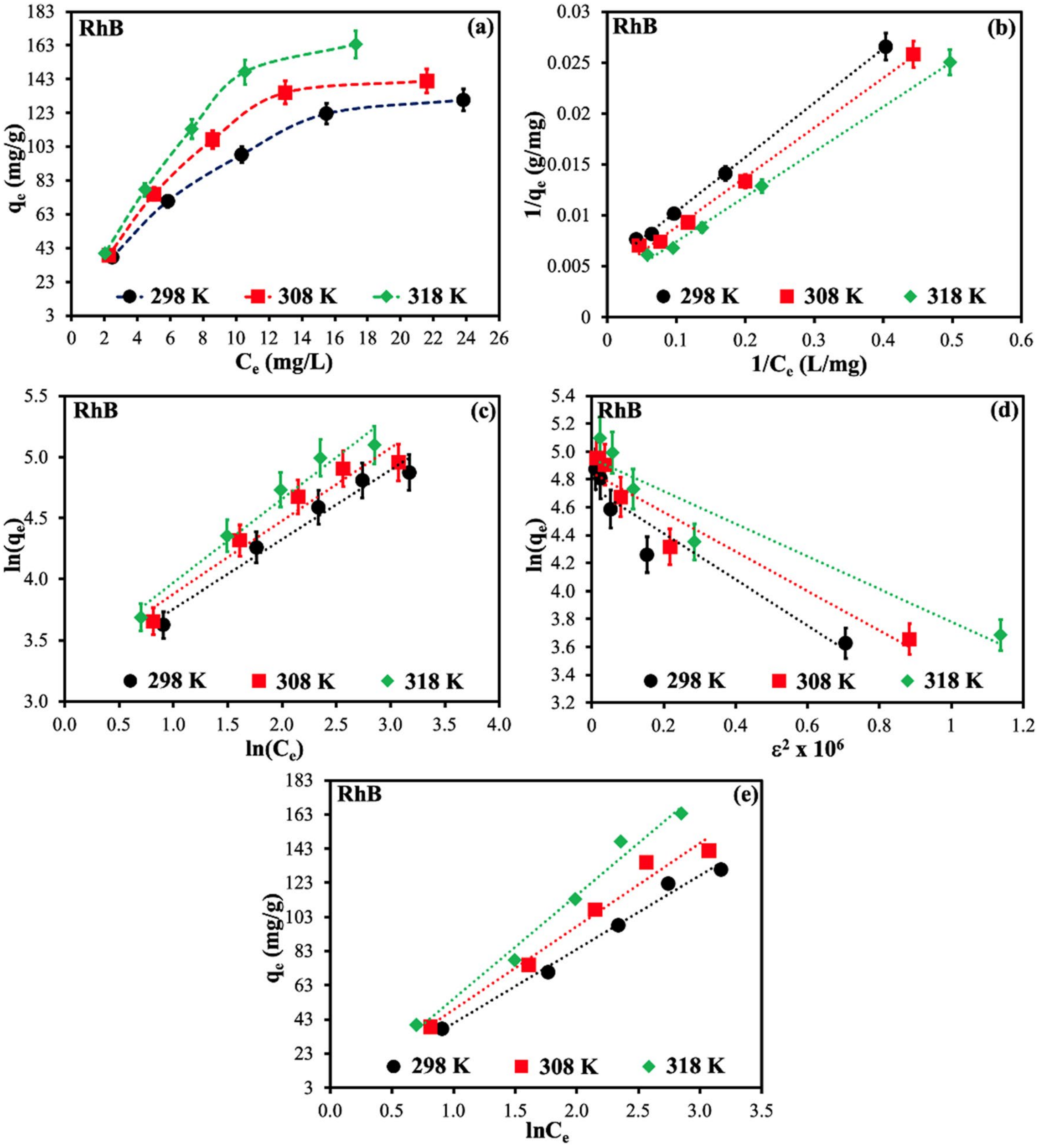

Fig. 6 Isotherm curves of RhB adsorption onto HP (**a**) and linear isotherm plots (constant dosage: 0.1 g, volume: 50 mL, contact time: 45 min, speed: 120 rpm, pH ≅ 7): Langmuir (**b**), Freundlich (**c**), D-R (**d**), and Temkin (**e**)

calculated as 0.55, 0.59, and 0.65 kJ/mol for 298, 308, and 318 K, which indicates that the process is physical for all temperatures. The Temkin isotherm disregards extremely low and extremely high concentrations and assumes that the heat of adsorption will decrease linearly as opposed to logarithmically. Furthermore, it assumes that bonding energy will be dispersed equally up to a specific maximum [46].

According to the r^2 values in Table 3, the order of isotherm feasibility was determined as Langmuir > Temkin > Freundlich > D-R. Furthermore, error analyses were performed between $q_{e,exp}$ and $q_{e,cal}$ values, and the results are depicted in Table 5. As seen in Table 5, it was observed that there was a similar order of fit between the isotherm models.

3.4 Adsorption kinetics and possible mechanism

To examine the kinetics of adsorption of RhB dye onto HP, *quasi-first-order* and *quasi-second-order* models were utilized [52, 53]. The linear equations are presented in Table 2. According to Table 2, time-dependent linear kinetic plots were plotted, and the results are shown in Fig. 7. The kinetic parameters and rate constants obtained from Fig. 7 are

Table 3 Isotherm parameters for the adsorption of RhB dye on HP (constant dosage: 0.1 g, volume: 50 mL, contact time: 45 min, speed: 120 rpm, pH ≅ 7)

	HP		
Temperature (K)	298	308	318
Freundlich isotherm			
K_F(mg/g).(L/g)$^{1/n}$	24.29	26.68	26.87
$1/n$	0.57	0.60	0.68
r^2	0.9680	0.9437	0.9669
Langmuir isotherm			
q_m(mg/g)	196.08	250.00	333.33
K_L(L/g)	0.0959	0.0821	0.0679
r^2	0.9990	0.9956	0.9978
Dubinin-Radushkevich isotherm			
q_{D-R}(mg/g)	114.90	127.68	141.25
E_{D-R}(kJ/mol)	0.55	0.59	0.65
r^2	0.9101	0.9263	0.9062
Temkin isotherm			
K_T(L/mg)	0.9446	1.001	0.9103
b_T(J/mol)	57.27	52.50	43.51
r^2	0.9885	0.9753	0.9822

Table 4 Summary of q_m values for RhB dye by various sorbents recorded in literature

Sorbent	q_m (mg/g)	Temp. (K)	Dose (g)	Ref.
HP	196.08	298	0.100	This study
Duolite C-20	28.571	208	0.400	[47]
Sodium montmorillonite	42.19	303	0.150	[48]
WAM	81.0	298	0.050	[49]
Biochar	238.42	298	0.035	[50]
Kaolinite	46.08	303	0.150	[51]

Table 5 Error functions for the adsorption of RhB dye on HP

	HP		
Temperature (K)	298	308	318
Freundlich			
SSE	399.1	934.9	869.2
ARE	7.969	11.13	8.868
RMSE	11.53	17.65	17.02
χ^2	3.327	7.046	5.640
EABS	37.99	57.82	53.15
Langmuir			
SSE	60.82	378.5	344.8
ARE	1.909	4.864	3.739
RMSE	4.503	11.23	10.72
χ^2	0.483	2.507	2.063
EABS	11.67	30.27	27.93
D-R			
SSE	860.7	875.9	1562
ARE	12.33	11.77	14.31
RMSE	16.94	17.09	22.82
χ^2	8.545	8.114	13.07
EABS	57.37	58.26	77.15
Temkin			
SSE	67.99	183.1	181.6
ARE	3.041	4.492	5.594
RMSE	4.761	7.811	7.780
χ^2	0.629	1.465	1.752
EABS	14.65	24.89	25.98

presented in Table 6. As seen in Table 6, it was observed that the adsorption of RhB dye on HP followed the *quasi-second-order* kinetic due to the r^2 values close to 1. Also, when $q_{e,exp}$ and $q_{e,cal}$ values were compared, it was found that the *quasi-second-order* kinetic was more appropriate. In addition, the error functions calculated between $q_{e,exp}$ and $q_{e,cal}$ values also proved that the *quasi-second-order* kinetic is more feasible for the process.

Figure 8 suggests the hypothesized adsorption mechanism of RhB dye on HP. As can be inferred from the FTIR-ATR spectra in Fig. 2, hydroxyl and carboxyl groups are present on the HP surface, and RhB dye is adsorbed onto the HP surface via electrostatic interaction with these functional groups and H-bonds.

Experimental investigations employing NaCl and $CaCl_2$ salts at various concentration levels were conducted in order to verify that the adsorption process is mediated by electrostatic interaction and to investigate the impact of different salt solutions on the adsorption process. Figure 9 presents the findings of an investigation into the impact of NaCl and $CaCl_2$ salts on the RhB adsorption process on HP. Figure 9 illustrates how an increase in salt concentrations causes the adsorption effectiveness of RhB dye to decrease. This is explained by the fact that the presence of $CaCl_2$ and NaCl protects the active sites on the adsorbent surface and raises the ionic strength of the aqueous medium. RhB dye molecules' electrostatic attraction to negatively charged active sites on the adsorbent surface may be weakened by the presence of positively charged Na^+ and Ca^{2+} ions in aqueous solutions, which may also lessen the negative charge of the active sites [54, 55].

3.5 Adsorption thermodynamics

Thermodynamic parameters for the adsorption of RhB dye on HP were found from the linear thermodynamic equations given in Table 2, and the results are presented in Fig. 10 and Table 7. As seen in Table 5, negative ΔH_A^S and ΔG_A^S values indicated that the process was exothermic (− 13.58 kJ/

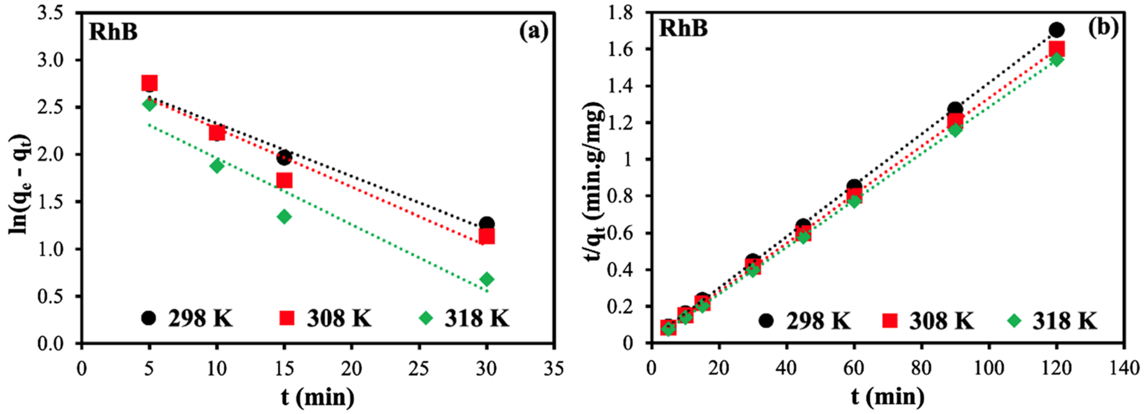

Fig. 7 The linear kinetic plots of RhB adsorption onto HP (constant dosage: 0.1 g, volume: 50 mL, concentration: 20 mg/L, speed: 120 rpm, pH ≅ 7): **a** *quasi-first-order* and **b** *quasi-second-order*

mol) and spontaneous (– 26.61 kJ/mol). The positive value (+43.74 kJ/mol) of ΔS_A^S indicated that the RhB molecules on the HP surface were more randomly arranged than in the solution.

3.6 Reusability experiments

A 0.1 M HCl solution was utilized for the reusability tests. Under ideal circumstances, adsorption and desorption investigations were conducted, and Fig. 11 shows the outcomes. Protons displace the RhB dye from the binding sites in an acidic solution. This makes sense since factors that affect regeneration include molecule size, contact point count, temperature, surface concentration, and the number of adsorbed species in the solution [56]. The adsorption effectiveness dropped from 72.32 to 49.87% after 5 cycles, according to the reusability experiments. The adsorbent's ability to effectively remove cationic dyes from aqueous solutions across multiple uses was demonstrated by these results.

Table 6 Kinetic parameters for the adsorption of RhB dye on HP (constant dosage: 0.1 g, volume: 50 mL, concentration: 20 mg/L, speed: 120 rpm, pH ≅ 7)

	HP		
Temperature (K)	298	308	318
Quasi-first-order			
k_1 (min^{-1})	0.0559	0.0619	0.0702
q_e (cal) (mg/g)	17.94	17.99	14.30
q_e (exp) (mg/g)	70.78	74.98	77.68
r^2	0.9653	0.9321	0.9238
SSE	2792	3247	4017
ARE	74.65	76.01	81.59
RMSE	30.51	32.90	36.59
χ^2	155.6	180.5	280.9
EABS	52.84	56.99	63.38
Quasi-second-order			
k_2 (g/mg.min)	0.0098	0.0101	0.0141
q_e (cal) (mg/g)	71.43	75.76	78.74
q_e (exp) (mg/g)	70.78	74.98	77.68
r^2	0.9998	0.9999	1.000
SSE	0.4225	0.6084	1.1236
ARE	0.9183	1.0402	1.3646
RMSE	0.3753	0.4503	0.6120
χ^2	0.0059	0.0080	0.0143
EABS	0.6500	0.7800	1.0600

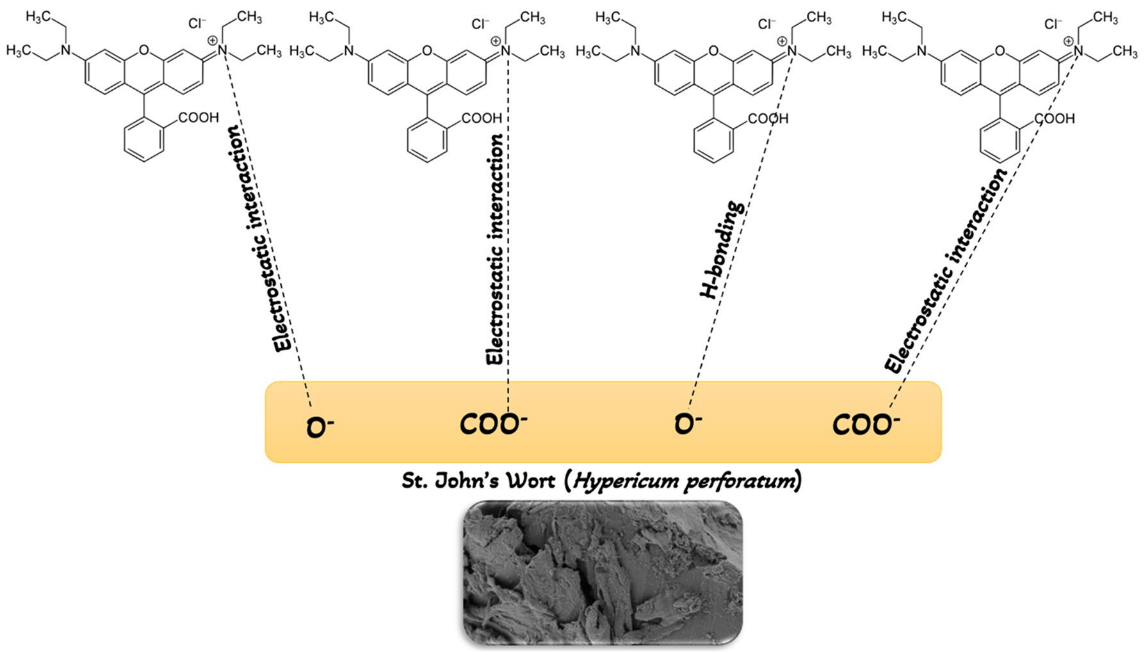

Fig. 8 The possible mechanism of RhB adsorption onto HP

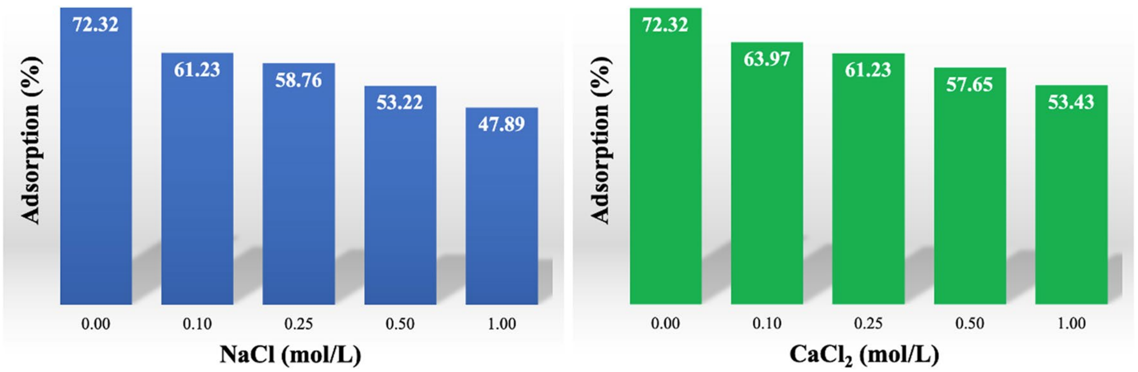

Fig. 9 The effect of salt concentration onto RhB adsorption on HP (constant dosage: 0.1 g, volume: 50 mL, concentration: 20 mg/L, speed: 120 rpm, pH ≅ 7)

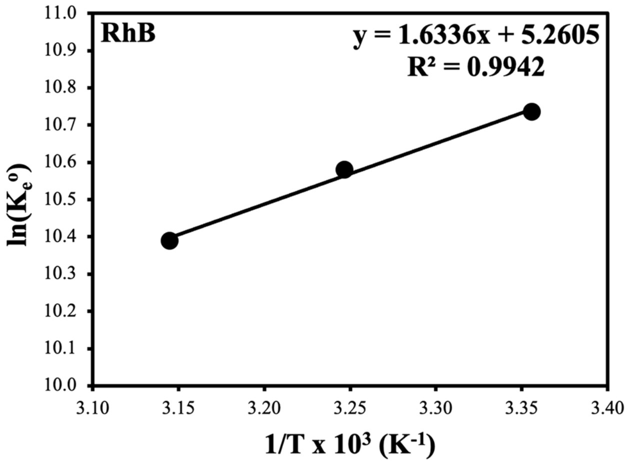

Fig. 10 The Van't Hoff plot of RhB adsorption onto HP (constant dosage: 0.1 g, volume: 50 mL, contact time: 45 min, speed: 120 rpm, pH ≅ 7)

Table 7 Thermodynamic parameters for adsorption of RhB dye on HP (constant dosage: 0.1 g, volume: 50 mL, contact time: 45 min, speed: 120 rpm, pH ≅ 7)

Thermodynamic parameters	ΔH^o_A (kJ/mol)	ΔS^o_A $(J/mol.K)$	ΔG^o_A(kJ/mol)		
			298 K	308 K	318 K
HP	− 13.58	43.74	− 26.61	− 27.05	− 27.49

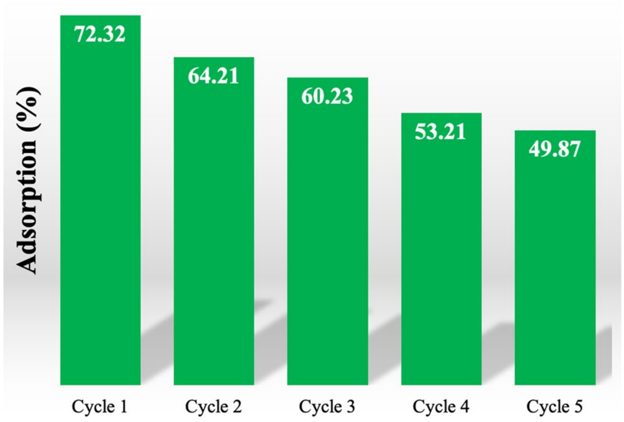

Fig. 11 The reusability of RhB adsorption onto HP (constant dosage: 0.1 g, volume: 50 mL, contact time: 45 min, speed: 120 rpm, pH ≅ 7)

4 Conclusions

In this work, HP was successfully utilized to obtain an efficient and low-cost adsorbent for the removal of RhB dye from wastewater. The characterization of HP was performed by FTIR-ATR, FESEM, XRD, and pH_{pzc} analyses. Additionally, post-adsorption FTIR-ATR and FESEM analyses were performed to investigate the evolution of the process. It was observed that pH played an important role in RhB removal and a superior interaction occurred at higher pH values. According to the r^2 values and error functions, the equilibrium data were found to best fit the Langmuir isotherm, and from this isotherm model the q_m value was calculated as 196.08 mg/g at 298 K. Kinetic tests illustrated that the process followed a *quasi-second-order* kinetic. This was also proved by error analysis. From the thermodynamic data, the removal of RhB on HP was found to be exothermic and spontaneous. Reusability studies showed that HP plant can be used repeatedly as a low-cost adsorbent for the removal of cationic dyes from aqueous solutions. All the results showed that HP could be an interesting and potential adsorbent for the effective removal of cationic pollutants from water for the development of low-cost and environmentally friendly adsorbents.

Supplementary information The online version contains supplementary material available at https://doi.org/10.1007/s13399-024-05840-7.

Author contribution Conceptualization: Birol Isik; methodology: Birol Isik; formal analysis and investigation: Birol Isik; writing—original draft preparation: Birol Isik; writing—review and editing: Birol Isik; resources: Birol Isik; supervision: Birol Isik.

Funding Open access funding provided by the Scientific and Technological Research Council of Türkiye (TÜBİTAK).

Data availability The data that support the findings of this study are available from the corresponding author upon reasonable request.

Declarations

Ethical approval Not applicable.

Competing interests The author declares no competing interests.

References

1. El-Nemr MA, Aigbe UO, Hassaan MA, Ukhurebor KE, Ragab S, Onyancha RB, Osibote OA, El Nemr A (2022) The use of biochar-NH_2 produced from watermelon peels as a natural adsorbent for the removal of Cu(II) ion from water. Biomass Convers Biorefin 14:1975–1991
2. Kusuma HS, Aigbe UO, Ukhurebor KE, Onyancha RB, Okundaye B, Simbi I, Ama OM, Darmokoesoemo H, Widyaningrum BA, Osibote OA, Balogun VA (2023) Biosorption of methylene blue using clove leaves waste modified with sodium hydroxide. Res Chem 5:100778
3. Akdemir M, Isik B, Cakar F, Cankurtaran O (2023) High-performing natural materials (*Leonurus cardiaca*): dye biosorption studies and statistical analysis. Biomass Convers Biorefin 13:14281–14299
4. Ukhurebor KE, Athar H, Adetunji CO, Aigbe UO, Onyancha RB, Abifarin O (2021) Environmental implications of petroleum spillages in the Niger Delta region of Nigeria: a review. J Environ Manage 293:112872
5. Ahamad Z, Ahmed M, Mashkoor F, Nasar A (2023) Chemically modified *Azadirachta indica* sawdust for adsorption of methylene blue from aqueous solutions. Biomass Convers Biorefin
6. Mashkoor F, Nasar A (2021) Environmental application of agro-waste derived materials for the treatment of dye-polluted water: a review. Curr Anal Chem 17:904–916
7. Jinendra U, Bilehal D, Nagabhushana BM, Kumar AP (2021) Adsorptive removal of rhodamine B dye from aqueous solution by using graphene–based nickel nanocomposite. Heliyon 7:e06851
8. Al-Gheethi AA, Azhar QM, Senthil Kumar P, Yusuf AA, Al-Buriahi AK, Mohamed RMSR, Al-shaibani MM (2022) Sustainable approaches for removing rhodamine B dye using agricultural waste adsorbents: a review. Chemosphere 287:132080
9. Imam SS, Babamale HF (2020) A short review on the removal of rhodamine B dye using agricultural waste-based adsorbents. Asian J Chem Sci 7:25–37
10. Rahdar S, Rahdar A, Zafar MN, Shafqat SS, Ahmadi S (2019) Synthesis and characterization of MgO supported Fe–Co–Mn nanoparticles with exceptionally high adsorption capacity for rhodamine B dye. J Mater Res Technol 8:3800–3810

11. Oyekanmi AA, Ahmad A, Hossain K, Rafatullah M (2019) Statistical optimization for adsorption of rhodamine B dye from aqueous solutions. J Mol Liq 281:48–58
12. Yen Doan TH, Minh Chu TP, Dinh TD, Nguyen TH, Vo TCT, Nguyen NM, Nguyen BH, Nguyen TA, Pham TD (2020) Adsorptive removal of rhodamine B using novel adsorbent-based surfactant-modified alpha alumina nanoparticles. J Anal Methods Chem 2020:1–8
13. Pham TD, Pham TT, Phan MN, Ngo TMV, Dang VD, Vu CM (2020) Adsorption characteristics of anionic surfactant onto laterite soil with differently charged surfaces and application for cationic dye removal. J Mol Liq 301:112456
14. Raji Y, Nadi A, Mechnou I, Saadouni M, Cherkaoui O, Zyade S (2023) High adsorption capacities of crystal violet dye by low-cost activated carbon prepared from Moroccan *Moringa oleifera* wastes: characterization, adsorption and mechanism study. Diam Relat Mater 135:109834
15. Teo SH, Ng CH, Islam A, Abdulkareem-Alsultan G, Joseph CG, Janaun J, Taufiq-Yap YH, Khandaker S, Islam GJ, Znad H, Awual R (2022) Sustainable toxic dyes removal with advanced materials for clean water production: a comprehensive review. J Clean Prod 332:130039
16. Alotaibi MT, Mogharbel RT, Alorabi AQ, Alamrani NA, Shahat A, El-Metwaly NM (2023) Superior adsorption and removal of toxic industrial dyes using cubic Pm3n aluminosilica form an aqueous solution, isotherm, kinetic, thermodynamic and mechanism of interaction. J Mol Liq 379:121672
17. Karadeniz SC, Ugraskan V, Isik B, Cakar F (2023) Mechanism and adsorptive performance of PANI/PTh copolymer as a novel and highly efficient adsorbent for the elimination of textile pollutants from aqueous solutions. Colloid Polym Sci 301:1209–1229
18. Ma X, Zhao S, Tian Z, Duan G, Pan H, Yue Y, Li S, Jian S, Yang W, Liu K, He S, Jiang S (2022) MOFs meet wood: reusable magnetic hydrophilic composites toward efficient water treatment with super-high dye adsorption capacity at high dye concentration. Chem Eng J 446:136851
19. Ouachtak H, El Haouti R, El Guerdaoui A, Haounati R, Amaterz E, Addi AA, Akbal F, Taha ML (2020) Experimental and molecular dynamics simulation study on the adsorption of rhodamine B dye on magnetic montmorillonite composite γ-Fe_2O_3@Mt. J Mol Liq 309:113142
20. Xiao W, Garba ZN, Sun S, Lawan I, Wang L, Lin M, Yuan Z (2020) Preparation and evaluation of an effective activated carbon from white sugar for the adsorption of rhodamine B dye. J Clean Prod 253:119989
21. Kumari S, Khan AA, Chowdhury A, Bhakta AK, Mekhalif Z, Hussain S (2020) Efficient and highly selective adsorption of cationic dyes and removal of ciprofloxacin antibiotic by surface modified nickel sulfide nanomaterials: kinetics, isotherm and adsorption mechanism. Colloids Surf Physicochem Eng Asp 586:124264
22. Ghibate R, Senhaji O, Taouil R (2021) Kinetic and thermodynamic approaches on rhodamine B adsorption onto pomegranate peel. Case Stud Chem Environ Eng 3:100078
23. Novera TM, Tabassum M, Bardhan M, Islam A, Islam A (2021) Chemical modification of betel nut husk prepared by sodium hydroxide for methylene blue adsorption. Appl Water Sci 11:66
24. Huck-Pezzei VA, Pallua JD, Pezzei C, Bittner LK, Schönbichler SA, Abel G, Popp M, Bonn GK, Huck CW (2012) Fourier transform infrared imaging analysis in discrimination studies of St. John's wort (*Hypericum perforatum*). Anal Bioanal Chem 404:1771–1778
25. Yontar AK, Avcioglu S, Cevik S (2022) Nature-based nanocomposites for adsorption and visible light photocatalytic degradation of methylene blue dye. J Clean Prod 380:135070
26. Jarzębski M, Smułek W, Baranowska HM, Masewicz L, Kobus-Cisowska J, Ligaj M, Kaczorek E (2020) Characterization of St. John's wort (*Hypericum perforatum* L.) and the impact of filtration process on bioactive extracts incorporated into carbohydrate-based hydrogels. Food Hydrocoll 104:105748
27. Dbik A, Bentahar S, El Khomri M, El Messaoudi N, Lacherai A (2020) Adsorption of Congo red dye from aqueous solutions using tunics of the corm of the saffron. Mater Today Proc 22:134–139
28. Rose PK, Kumar R, Kumar R, Kumar M, Sharma P (2023) Congo red dye adsorption onto cationic amino-modified walnut shell: characterization, RSM optimization, isotherms, kinetics, and mechanism studies. Groundw Sustain Dev 21:100931
29. Watwe V, Kulkarni S, Kulkarni P (2023) Development of dried uncharred leaves of *Ficus benjamina* as a novel adsorbent for cationic dyes: kinetics, isotherm, and batch optimization. Ind Crops Prod 195:116449
30. Mosoarca G, Vancea C, Popa S, Dan M, Boran S (2023) A novel high-efficiency natural biosorbent material obtained from sour cherry (*Prunus cerasus*) leaf biomass for cationic dyes adsorption. Mater 16:4252
31. Sismanoglu S, Akalin MK, Akalin GO, Topak F (2023) Effective removal of cationic dyes from aqueous solutions by using black cumin (*Nigella sativa*) seed pulp and biochar. BioResources 18:3414–3439
32. Isik B, Avci S, Cakar F, Cankurtaran O (2023) Adsorptive removal of hazardous dye (crystal violet) using bay leaves (*Laurus nobilis* L.): surface characterization, batch adsorption studies, and statistical analysis. Environ Sci Pollut Res 30:1333–1356
33. Ivanova L, Vassileva P, Detcheva A (2020) Characterization and adsorption properties of *Hypericum perforatum* L. for the removal of Cu^{2+} ions from aqueous solutions. Cellulose Chem Technol 54:1023–1030
34. Deng H, Mao Z, Xu H, Zhang L, Zhong Y, Sui X (2019) Synthesis of fibrous $LaFeO_3$ perovskite oxide for adsorption of rhodamine B. Ecotoxicol Environ Saf 168:35–44
35. Akin K, Ugraskan V, Isik B, Cakar F (2022) Adsorptive removal of crystal violet from wastewater using sodium alginate-gelatin-montmorillonite ternary composite microbeads. Int J Biol Macromol 223:543–554
36. Vigneshwaran S, Sirajudheen P, Karthikeyan P, Meenakshi S (2021) Fabrication of sulfur-doped biochar derived from tapioca peel waste with superior adsorption performance for the removal of Malachite green and rhodamine B dyes. Surf Interf 23:100920
37. Karadeniz SC, Isik B, Ugraskan V, Cakar F (2023) Adsorptive removal of safranine T dye from aqueous solutions using sodium alginate–*Festuca arundinacea* seeds bio–composite microbeads. Int J Biol Macromol 248:125880
38. Firoozi M, Rafiee Z, Dashtian K (2020) New MOF/COF hybrid as a robust adsorbent for simultaneous removal of auramine O and rhodamine B dyes. ACS Omega 5:9420–9428
39. Cui W, Kang X, Zhang X, Cui X (2019) Gel-like ZnO/Zr-MOF(bpy) nanocomposite for highly efficient adsorption of rhodamine B dye from aqueous solution. J Phys Chem Solids 134:165–175
40. Zhao Z, Yao L, Li J, Ma X, Han L, Lin Z, Guan S (2022) Determination of interactions of ferrihydrite-humic acid-Pb (II) system. Environ Sci Pollut Res 29:21561–21575
41. Zhao Z, Yao L, Li J, Ma X, Han L, Lin Z, Guan S (2022) Correction to: Determination of interactions of ferrihydritehumic acid Pb (II) system. Environ Sci Pollut Res 29:21576–21576
42. El Haouti R, Ouachtak H, El Guerdaoui A, Amedlous A, Amaterz E, Haounati R, Addi AA, Akbal F, El Alem N, Taha ML (2019) Cationic dyes adsorption by Na-montmorillonite nano clay: experimental study combined with a theoretical investigation using DFT-based descriptors and molecular dynamics simulations. J Mol Liq 290:111139

43. Duran H, Sismanoglu S, Sismanoglu T (2019) Binary biomaterials (inorganic material/natural resin): synthesis, characterization and performance for adsorption of dyes. J Ind Chem Soc 96:1245–1251
44. Isik B, Ugraskan V, Cankurtaran O (2022) Effective biosorption of methylene blue dye from aqueous solution using wild macrofungus (*Lactarius Piperatus)*. Sep Sci Technol 57:854–871
45. Nazir MA, Najam T, Jabeen S, Wattoo MA, Bashir MS, Shah SSA, Rehman A (2022) Facile synthesis of tri-metallic layered double hydroxides (NiZnAl-LDHs): adsorption of Rhodamine-B and methyl orange from water. Inorg Chem Commun 145:110008
46. Inyinbor AA, Adekola FA, Olatunji GA (2016) Kinetics, isotherms and thermodynamic modeling of liquid phase adsorption of rhodamine B dye onto *Raphia hookerie* fruit epicarp. Water Resour Ind 15:14–27
47. Al-Rashed SM, Al-Gaid AA (2012) Kinetic and thermodynamic studies on the adsorption behavior of rhodamine B dye on Duolite C-20 resin. J Saudi Chem Soc 16:209–215
48. Selvam PP, Preethi S, Basakaralingam P, Thinakaran N, Sivasamy A, Sivanesan S (2008) Removal of rhodamine B from aqueous solution by adsorption onto sodium montmorillonite. J Hazard Mater 155:39–44
49. Postai DL, Demarchi CA, Zanatta F, Melo DCC, Rodrigues CA (2016) Adsorption of rhodamine B and methylene blue dyes using waste of seeds of *Aleurites Moluccana*, a low cost adsorbent. Alexandria Eng J 55:1713–1723
50. Albanio II, Muraro PCL, da Silva WL (2021) Rhodamine B dye adsorption onto biochar from olive biomass waste. Water Air Soil Pollut 232:214
51. Khan TA, Dahiya S, Ali I (2012) Use of kaolinite as adsorbent: equilibrium, dynamics and thermodynamic studies on the adsorption of rhodamine B from aqueous solution. Appl Clay Sci 69:58–66
52. Anandkumar J, Mandal B (2011) Adsorption of chromium(VI) and rhodamine B by surface modified tannery waste: kinetic, mechanistic and thermodynamic studies. J Hazard Mater 186:1088–1096
53. Bilgi M, Ugraskan V, Isik B (2023) Biosorption studies of methylene blue dye using NaOH-treated *Aspergillus niger* -filled sodium alginate microbeads. Chem Eng Commun 210(9):1405–1419
54. da Silva JS, da Rosa MP, Beck PH, Peres EC, Dotto GL, Kessler F, Grasel FS (2018) Preparation of an alternative adsorbent from *Acacia Mearnsii* wastes through acetosolv method and its application for dye removal. J Clean Prod 180:386–394
55. salah omer A, Naeem AE, Abd-Elhamid G, Farahat AI, El-Bardan OOM, Soliman AA, Nayl HMA AA (2022) Adsorption of crystal violet and methylene blue dyes using a cellulose-based adsorbent from sugercane bagasse: characterization, kinetic and isotherm studies. J Mater Res Technol 19:3241–3254
56. Bello OS, Alabi EO, Adegoke KA, Adegboyega SA, Inyinbor AA, Dada AO (2020) Rhodamine B dye sequestration using *Gmelina aborea* leaf powder. Heliyon 6:e02872